TITLE: Application of Pyrometry and IR-Thermography to High Surface Temperature Measurements

Application of Pyrometry and IR-Thermography to High Surface Temperature Measurements

A. Gülhan
German Aerospace Center (DLR)
Institute of Fluid Mechanics
Wind Tunnel Division in Cologne
Porz-Wahnheide, Linder Höhe
D-51147 Cologne, Germany

Summary

In this document the non-intrusive temperature measurement techniques like pyrometry and IR-thermography and their application at high temperatures are described. For a better understanding first some basic relations of thermal radiation are discussed followed by the absorption behaviour of the atmosphere and optical glasses. Main properties of different IR detector types follows this chapter. Chapters five and six are devoted to the description of pyrometers and IR-cameras including a comparison of different detectors, data reduction and imaging techniques. Based on the experience from application of IR devices at the arc heated facility LBK, some requirements on an IR-system for its use at high enthalpy facilities are defined. Results of comparative and complementary measurements of the surface temperature of several thermal protection materials using pyrometers and IR-cameras are presented in chapter nine.

1. List of symbols

A	surface area
CCD	charge coupled device
C-SiC	carbon fibre reinforced silicon carbide
c	speed of light in vacuum
c_1, c_2	radiation constants
D	detectivity
d	distance
E	energy
FPA	focal plane array
h	Planck's constant
I	photo current
IR	infrared
k	Boltzmann's constant
L	radiant intensity
LBK	arc heated facility of DLR
L_λ	spectral radiance
NEP	noise equivalent power
R	reflectance
r	radius
SiC	silicon carbide
T	temperature
TPS	thermal protection system
W	radiance
α	absorption coefficient
ε	emissivity
Φ	radiant flux
λ	wavelength
τ	transmittance
ν	frequency
Ω	solid angle

Subscripts

b	black body
cal	calibration
D	detector
F	filter
G	geometric
M	media
m	measured
O	optics
p	primary
S	stop
s	secondary
t	total

Paper presented at the RTO AVT Course on "Measurement Techniques for High Enthalpy and Plasma Flows", held in Rhode-Saint-Genèse, Belgium, 25-29 October 1999, and published in RTO EN-8.

2. Introduction

The measurement of the surface temperature of test models in high enthalpy and hypersonic flows has been a big challenge for engineers. Because of chemical reactions between the solid and gas phases at high temperatures, mechanical temperature sensors like thermocouples, thermo-resistance sensors, etc. find only a limited application in such environments. In these cases and some other applications, where mechanical sensors can disturb the flow field as a result of interaction with the supersonic flow, non-intrusive temperature measurement techniques provide more reliable data. These techniques find a broad application in rotating systems as well.

IR-thermography and pyrometry are two well developed non-intrusive techniques for the measurement of the surface temperature. Because of their relatively simpler hardware, and lower costs mostly pyrometers are used for the measurement of local surface temperatures up to 3000°C. A simultaneous surface temperature distribution, which is sometimes essential for the interpretation of physical phenomena, can only be measured with more complex IR-cameras. Parallel to the developments in electronics and materials for optical components significant progress has been made recently with respect to the temperature resolution, quick response and good accuracy of IR-devices.

In this document, basic relations of thermal radiation, the properties of IR components and different applications of pyrometers and IR-cameras will be discussed.

3. Basic relations of thermal radiation

Each object at a temperature of higher than absolute zero emits light in the visible and infrared wavelength ranges. The glowing of materials heated to temperatures above 500°C is the optical manifestation of this radiation. The change in colour of the emitted light with increasing temperature shows the dependence of thermal radiation on wavelength.

Some main parameters of the thermal radiation are defined below [1]:

The radiant flux Φ is the radiance dW emitted during a time duration dt into a hemisphere:

$$\Phi = dW / dt \ [\mathrm{W/m^2}]. \qquad (1)$$

Consider a radiation source element A_1 and a detector element A_2 in a hemispherical optical space **(Fig. 1)**.

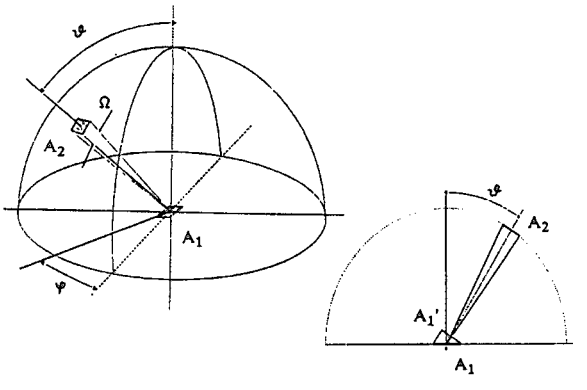

Figure 1. Beam geometry in a hemispherical space

Let Ω be the solid angle subtended by A_2 at A_1. We then have:

$$\Omega = A_2 / r^2 \left[m^2 / m^2 \triangleq Steradiant \right]. \qquad (2)$$

Using the above mentioned parameters Φ and Ω the radiant intensity can be derived as:

$$L = \frac{d^2\Phi}{dA_1 \cdot d\Omega \cdot \cos\Theta}\left[W/m^2 \cdot sr\right]. \quad (3)$$

Since only a limited spectral range of radiation is used in IR-thermography, it is necessary to introduce the spectral radiance (intensity) L_λ:

$$L_\lambda = \frac{dL}{d\lambda} = \frac{d^3\Phi}{dA_1 \cdot d\Omega \cdot d\lambda \cdot \cos\Theta}. \quad (4)$$

In order to keep the surface energy of an arbitrary body exposed to radiation constant, the sum of the reflected, absorbed and transmitted parts of light must equal the incident radiant intensity. The absorption coefficient α, reflectance R and transmission factor τ of a body are defined as:

$$\alpha = L_{\lambda_{absorbed}} / L_{\lambda_{total}} \quad (5)$$

$$R = L_{\lambda_{reflected}} / L_{\lambda_{total}} \quad (6)$$

$$\tau = L_{\lambda_{transmitted}} / L_{\lambda_{total}}. \quad (7)$$

The condition of constant energy leads to the following relation

$$\alpha + R + \tau = 1. \quad (8)$$

In general, these three parameters are functions of the temperature T, the wavelength λ, the azimuth angle φ and the zenith angle Θ of the radiation:

$$\begin{aligned} \alpha &= \alpha(T, \lambda, \varphi, \Theta) \\ R &= R(T, \lambda, \varphi, \Theta). \\ \tau &= \tau(\lambda, T, \varphi, \Theta) \end{aligned} \quad (9)$$

There are no reliable theoretical relations to describe the dependence on all these parameters. A sophisticated and very complex set-up is necessary to investigate this problem experimentally. Only for special conditions, like for a black body, can the dependence between different radiation parameters be expressed analytically. A black body absorbs the incident light totally. This means the absorption coefficient α is independent of temperature, wavelength and light incident angles and has the value $\alpha = 1$, i.e. $R = \tau = 0$. A cavity surrounded with a cylindrical or spherical body with nontransmittive walls in thermal equilibrium is a common black body. Kirchhoff experimentally found that the ratio of the absorption coefficient α and emission coefficient ε of an arbitrary surface has a constant value 1 (Kirchhoff's law):

$$\alpha / \varepsilon = 1. \quad (10)$$

According to the Kirchhoff's law the spectral radiance of an arbitrary surface L_λ is a product of its emissivity ε and the radiant intensity of a black body L_{λ_b}:

$$L_\lambda = \varepsilon \cdot L_{\lambda_b}. \quad (11)$$

The emissivity of a surface also depends on the temperature and the wavelength (the influence of angles φ and Θ is weak and neglected here):

$$\varepsilon = \varepsilon(\lambda, T). \quad (12)$$

Based on quantum mechanics Planck analytically derived the following equation to describe the spectral radiance of a black body (Planck's law):

$$L_{\lambda_b}(\lambda,T)=\frac{c_1}{\Omega\pi\lambda^5}\cdot\frac{1}{e^{c_2/(\lambda\cdot T)}-1} \qquad (13)$$

where

$c_1 = 2\pi c^2 h = 3.7414\cdot 10^{-16}$ [Wm²]

$c_2 = ch/k = 1.4388\cdot 10^{-2}$ [mK]

and

$c = 2.997925\cdot 10^{8}$ [m/s]	the speed of light in vacuum
$h = 6.6256\cdot 10^{-34}$ [J s]	the Planck's constant
$k = 1.38054\cdot 10^{-23}$ [J/K]	the Boltzmann's constant

are universal constants.

Thus, the thermal emission of a real body can be described by the following equation:

$$L_\lambda(\lambda,T)=\varepsilon(\lambda,T)\frac{c_1}{\Omega\pi\lambda^5}\cdot\frac{1}{e^{c_2/(\lambda\cdot T)}-1}\,. \qquad (14)$$

For temperatures up to about 2700 K:

$$\lambda T << c_2,\ i.e.,\ e^{c_2/(\lambda\cdot T)} >> 1. \qquad (15)$$

Thus, the Planck's equation can be approximated by the Wien's equation:

$$L_\lambda(\lambda,T)=\varepsilon(\lambda,T)\frac{c_1}{\Omega\pi\lambda^5}\cdot e^{-c_2/(\lambda\cdot T)}\,. \qquad (16)$$

This equation shows good agreement with the Planck's law within an accuracy of 0.1% and can therefore be applied at low temperatures.

The temperature of a real surface can be determined using the definition of a "black temperature" $T_b(\lambda)$. $T_b(\lambda)$ is the temperature of a black body, which at the wavelength λ has the same radiance as the real surface

$$L_\lambda(\lambda,T)=L_{\lambda,b}(\lambda,T_b(\lambda)) \qquad (17)$$

where T is the "true temperature" of the real surface. Planck's law leads to

$$\frac{1}{T}=\frac{1}{T_b}+\frac{\lambda}{c_2}ln\,\varepsilon(\lambda,T)-\frac{\lambda}{c_2}ln\frac{1-e^{-c_2/(\lambda\cdot T)}}{1-e^{-c_2/(\lambda\cdot T_b(\lambda))}}\,. \qquad (18)$$

Using the black temperature, which can be determined from the spectral intensity directly, the temperature of the real body with the same radiance can be calculated using eq. (18).

In practical applications, however, the influence of the measurement environment on the components of the IR-device have to be taken into account for a reliable temperature measurement.

4. Optical components of pyrometers and IR-cameras

IR-devices use mainly quantum or thermal detectors and provide photo currents as output signals, which are correlated to the intensity of the emitted light. A principal set-up is shown in **Fig. 2.**

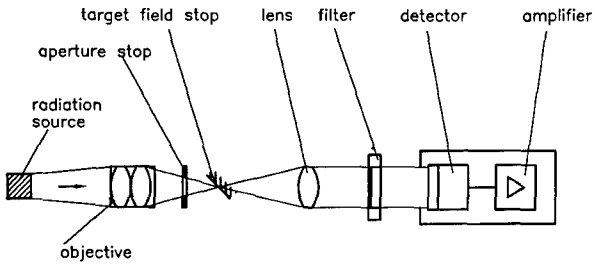

Figure 2. Main components of an IR-device

4.1 Aperture and field stops

Any element, be it the rim of a lens or a separate diaphragm, which determines the amount of light passing it, is called an aperture stop. At the same time it prevents the light emitted from foreign objects from entering the pyrometer. However highly oblique rays can still enter a system of this sort. Further improvement can be reached using a field stop, which determines the field of view of the instrument.

The spectral response of an IR-device is determined by the spectral behaviour of all its optical and opto-electronic components, i.e. the spectral transmittance of the medium, optical lenses, optical filters and the spectral response of the radiation detector.

4.2 Absorption of thermal radiation by the atmosphere

The atmosphere between the radiation source and the detector can partly absorb the emitted light and cause perturbations in temperature measurement. The transmission of optical radiation by the atmosphere depends mainly on two phenomena: self-absorption by the gas species and deflection due to scattering of the light by particles in the gas atmosphere.

Figure 3 shows the transmission spectrum of the air atmosphere for the given distance under well-defined weather conditions [2]. Since the thermal radiation at temperatures up to 3000°C mainly occurs in the near and middle infrared spectral range, the transmittance τ_M of atmospheric air in this region is important for IR-measurements. Water vapour in air has strong absorption bands in the infrared spectrum. The main absorption bands due to water vapour lie at about 2.6 µm and between 5.5 µm and 7.5 µm. This fact has to be considered in the frame of the characterization of spectral properties of a IR-devices. Compared to water vapour, the absorption of infrared radiation due to carbon dioxide (CO_2) is weaker. Other species in atmospheric air have negligible influence on the transmission of the air for infrared radiation.

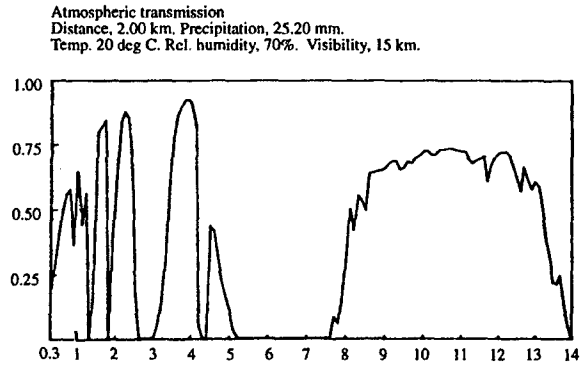

Figure 3. Spectral transmittance of air atmosphere [2]

4.3 Optical glasses and filters

Beside its optical properties the physical characteristics of an optical system are to be taken into account for its specification. The manufacturing and optical polishing of glasses is only possible above a certain hardness. Another important factor is the matching of optical glasses and their support sys-

tems in terms of their thermal expansion behaviour. Additionally their resistance to physical abrasion and chemical corrosion must be high.

Most optical glasses are not transparent beyond about 3 μm because of strong absorption by OH-ions. Fused quartz or fused silica glasses transmit satisfactorily up to 5 μm. Absorption above this limit is caused due to the vibration of the Si-O band. During the fabrication of glasses particular care is necessary to avoid any water diffusion into the glass, since, as previously shown, water vapour has strong absorption lines in this spectral range. Some special glasses, due to their material properties or fabrication processes can transmit in a much broader spectrum (**Fig. 4**).

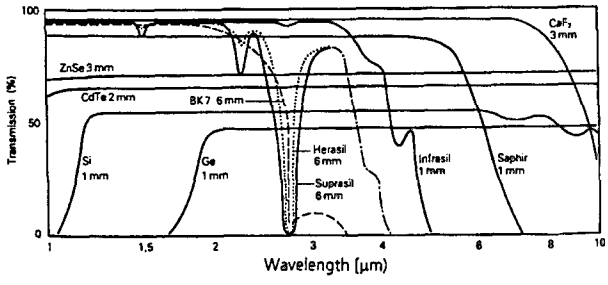

Figure 4. Transmittance of different optical glasses

The transmittance of glasses with highly reflective surfaces can be improved by the deposition of an anti-reflective thin film. Using multilayer anti-reflective coatings the reflectance can be reduced (i.e. the transmittance can be increased over a wider spectral range).

Depending on the spectral properties of the detector, different types of filters can be used, in order to provide well-defined spectral intervals of the radiative beam reaching the detector. Low pass filters absorb the light at wavelengths beyond a certain wavelength. High pass filters are transparent only at wavelengths beyond a certain limit. Band-pass filters can be considered as a combination of both these filters and transmit only in a defined wavelength interval. High selectivity can be achieved by means of interference filters. These filters consist of a transparent material with a multilayer surface coating. To achieve strong interference between incident and reflected waves, high reflectivity at the interface is required. Multilayer surface coating of alternate films with high and low refraction indices (mostly metal - dielectric-metal films) provide high and selective reflectance.

4.4 Detectors

A radiation detector transforms electromagnetic radiation into an electrical signal. There are two basic types of detector: thermal detectors and quantum detectors.

4.4.1 Thermal detectors

Thermal detectors change their energy level, i.e. temperature, due to absorption of the incident radiation flux. These do not respond to photons but to radiant flux. The output signal of the detector is proportional to the temperature change and is independent of the wavelength.

Bolometers are thermal detectors in which the incident radiation produces a change in the temperature, i.e. in resistance of the sensitive surface (**Fig. 5**) [3]. Due to the constant voltage across the bolometer surface this resistance change leads to a current change. Compared to quantum detectors the response time of bolometers is remarkably longer

(several milliseconds). Metals or semiconductors are used as bolometer materials. The fact that bolometers can be used without detector cooling makes them very interesting for several applications.

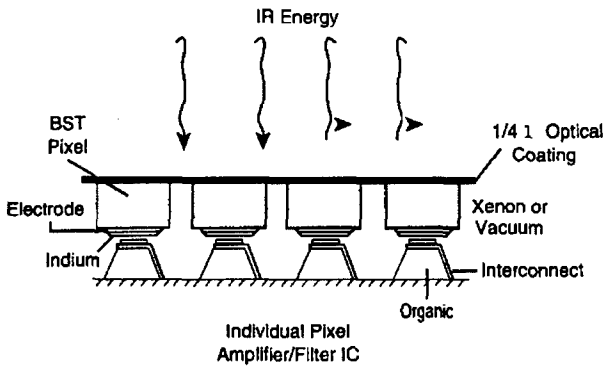

Figure 5. Bolometer detector [3]

Thermopiles consisting of several thermocouples, which are connected in series, are also used in IR-devices. As it is known, heating of one junction of a thermocouple compared to other one produces a voltage across the thermoelement. The multijunction of thermopiles allows to achieve sufficient signal even at low heating rates. Thermopiles do not need energy input and therefore find application in IR-systems of satellites.

Pneumatic thermal detectors use the effect of pressure change in a gas chamber due to radiation heating. Two chambers are separated by a membrane and have a capillary connection for pressure equilibrium. The radiance absorption through a sensitive element in the first chamber causes a pressure increase, i.e. deformation of the membrane. It changes electrostatic capacitance of a condenser, which use the membrane as one of the electrodes. Some pneumatic detectors use optical interference method instead of condenser technique.

4.4.2 Quantum detectors

Quantum detectors measure the direct excitation of electrons to conduction states by incident photons and are also called photo-electric detectors. There are different types of photo-electric detectors.

Photo emissive detectors consist of a metal photo cathode at a negative voltage and an anode at a positive voltage level. Both electrodes are integrated in an evacuated glass tube. If the energy of incident photons is higher than the electron band energy, they leave the cathode and accelerate to the anode in the vacuum and create a current. The spectral sensitivity of these detectors depends on the optical properties of the photo cathode. Some photo emissive detectors, so-called photo multipliers, consist of a set of electrodes (dynodes), each of them held at a different potential. Each electron colliding with a dynode produces new electrons, which accelerates to the next dynode like a chain reaction and a large number of electrons reach the anode. Photo emissive detectors are sensitive in the ultraviolet, the visible and the near infrared spectra.

The second group of quantum detectors is based on the change of the conductivity of the detector by absorbing photons. In some materials, like semiconductors, electrons excited by the photons do not leave the material but jump to another energy level. At absolute zero temperature, electrons occupy the lowest energy levels in a band called the valence band (**Fig. 6**). When the electrons absorb sufficient energy they can jump to the highly energetic con-

ductive band after passing the forbidden Fermi level. This process is coupled with current creation between those two regions of the material. The difference between the conduction band energy and valence band energy is called the activation energy. If the activation energy of the material is smaller than the energy $h\nu$ of the incident photon, sufficient electrons can cross the forbidden band and the material becomes conductive. These types of materials are called intrinsic semiconductors (PbS, InSb, HgCdTe, etc.). The conductivity of a semiconductor can be increased by doping some foreign particles with different valence levels. The application of photo conductive detectors is restricted by the recombination noise due to the electron-hole pairs by absorption of radiation.

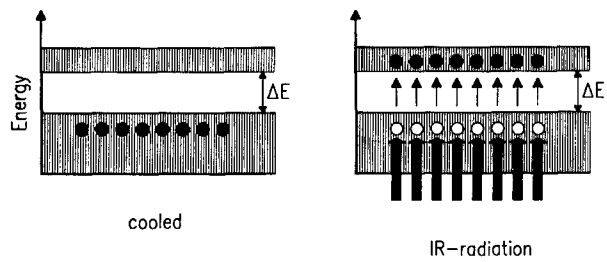

Figure 6. Photoconductive detector.

In the case of photovoltaic detectors, the photon absorption changes the potential distribution in the junction area of an inhomogeneous semiconductor. The local change of the electrical field E due to the junction distorts the conduction and valence bands between the n and p regions. The absorption of photons, with sufficient energy, release some electrons and holes which then diffuse across the junction under the influence of the field E and create a current. Photo-electric detectors behave as energy generators and can produce signals even in the absence of bias. Photo voltaic detectors have a faster response than photo conductive detectors. The photo voltaic effect is widely used in photo diodes, photo transistors and infrared detectors such as InAs, InSb and TeCdMg. These types of detectors have a lower noise level than photo conductors. The diffusion of electrons and holes prevents recombination.

4.4.3 Detector cooling

The main advantage of thermal detectors is their operation without active cooling. Depending on the application this aspect could be essential. In contrary quantum detectors has to be cooled to achieve a good signal to noise ratio. Each detector has a permanent noise level resulting from the thermal vibrations and the particle nature of light and electricity. The signal power equal to the noise power of the detector is called the noise equivalent power (NEP). It strongly depends on the temperature. The detectivity of a detector D is inversely proportional to the NEP. **Figure 7** shows the detectivity of some detectors at different temperature levels. By reducing the temperature from 295 K to 193 K or 77 K, the noise level can be decreased, i.e. the detectivity can be improved.

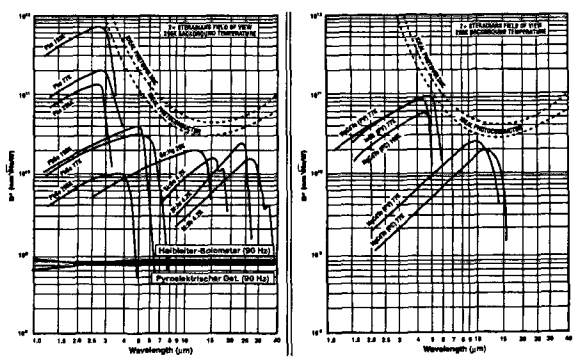

Figure 7. Spectral detectivity of different detectors [4]

Depending on the required temperature level, different types of systems can be used for detector cooling: Liquefied gas, Joule-Thomson expansion, cryogenic machines and thermoelectric techniques. Liquid nitrogen keeps the temperature constant at 77 K and is widely used in IR-thermography. The Joule-Thomson effect is used for cooling to temperatures below about 150 K [2]. The thermoelectric technique is applied in a temperature range between 160 K and 320 K. The Peltier thermoelectric effect is the result of the absorption or release of heat at the junction of two different metals with an electrical current flowing across it. In practical applications, a side from the Peltier effect, the thermal conductivity of metals and Joule heating of conductors, which are proportional to the resistance of the metals have to be taken into account.

5. Pyrometer technique

Because of their relatively easier imaging and signal processing compared to IR-cameras pyrometers find a broad application in the measurement of local temperatures on objects. Spectral pyrometers and total radiation pyrometers have nearly the same set-up, except for different characteristics of the filter and detector. A typical pyrometer set-up is shown in **Fig. 8**. The spectral transmittance of the filter and the spectral detector response have to match in the chosen wavelength interval.

In general, the radiance emitted by the radiation source can arrive at the detector directly or along other paths due to reflection from foreign objects (R_k) (**Fig. 9**). In addition the radiance of some other light sources or daylight L_{λ_E} has to be taken into account. The radiation intensity decreases according to the transmittance of surrounding media τ_M, lenses τ_0, filter τ_F or stop τ_G before reaching the detector.

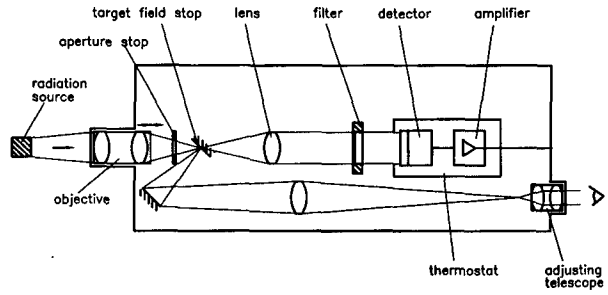

Figure 8. Set-up of a spectral pyrometer

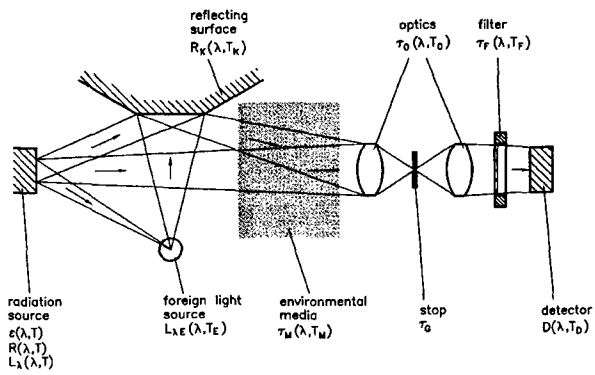

Figure 9. Beam path of a spectral pyrometer

If we neglect multiple reflections, the temperature dependence of the reflectance and transmittance of the components, the total radiance can then be expressed by:

$$L_{\lambda,} = \tau_M(\lambda)\cdot\tau_0(\lambda)\cdot\tau_F(\tau)\cdot\tau_G \cdot\begin{bmatrix} L_\lambda(\lambda,T)\cdot(1+R_k(\lambda))+ \\ L_{\lambda_E}(\lambda,T_E)\cdot(1+R(\lambda,T)+R_k(\lambda)) \end{bmatrix} \quad (19)$$

or it can be written in another form:

$$L_{\lambda,} = \tau_M(\lambda)\cdot\tau_0(\lambda)\cdot\tau_F(\lambda)\cdot\tau_G \cdot\left[L_{\lambda_p}(\lambda,T)+L_{\lambda_s}(\lambda,T_E)\right] \quad (20)$$

where

$$L_{\lambda_p}(\lambda,T)=L_{\lambda}(\lambda,T)\cdot(1+R_k(\lambda))$$

$$L_{\lambda_s}(\lambda,T_E)=L_{\lambda_E}(\lambda,T_E)\cdot(1+R(\lambda,T)+R_k(\lambda)).$$

The spectral radiance of the radiation source $L_{\lambda}(\lambda,T)$ and foreign light sources $L_E(\lambda,T_E)$ are defined by the eq. (14) and (16).

The effective radiance at the detector surface is:

$$L_D=\int_{\lambda_1}^{\lambda_2}\tau_M(\lambda)\cdot\tau_0(\lambda)\cdot\tau_F(\lambda)\cdot\tau_G \cdot\left[L_{\lambda_p}(\lambda,T)+L_{\lambda_s}(\lambda,T_E)\right]d\lambda \quad (21)$$

The detector itself is characterized by its spectral detectivity $D(\lambda,T_D)$. Since its temperature is usually kept at a constant level, the temperature dependence can be neglected.

The signal of the detector I_D is:

$$I_D=\int_{\lambda_1}^{\lambda_2}\tau_G\cdot\tau_M(\lambda)\cdot\tau_0(\lambda)\cdot\tau_F(\lambda) \cdot\left[L_{\lambda_p}(\lambda,T)+L_{\lambda_s}(\lambda,T_E)\right]D(\lambda)\cdot d\lambda \quad (22)$$

In practical applications, it is very difficult to describe all parameters as a function of wavelength analytically.

The most efficient way to overcome this problem is to use the linear range of a detector, where the output signal current is proportional to the incident light intensity. After accounting for the optical system of the pyrometer, the current and radiance ratios can be equated as follows:

$$\frac{I_{D_1}}{I_{D_2}}=\frac{L_{D_1}}{L_{D_2}} \quad (23)$$

Since spectral pyrometers use a narrow wavelength interval, one can write using Planck's equation:

$$\frac{I_{D_1}}{I_{D_2}}=\frac{L_{D_1}}{L_{D_2}}=\frac{e^{c_2/(\lambda_{1,2}\cdot T_2)}-1}{e^{c_2/(\lambda_{1,2}\cdot T_1)}-1} \quad (24)$$

where $\lambda_{1,2}$ is the "mean effective wavelength" of the system relating to temperatures T_1 and T_2 of a black body. The temperature T_2 can be expressed as follows:

$$T_2=\frac{c_2/\lambda_{1,2}}{ln\left[\frac{I_{D_1}}{I_{D_2}}\left(e^{c_2/(\lambda_{1,2}\cdot T_1)}-1\right)+1\right]} \quad (25)$$

The data I_{D_1} and T_1 are determined by measuring the photo current of the detector $I_{D_1}=I_{cal}$ at a black body of known temperature of $T_1=T_{cal}$ as a reference point. Using eq. (25) for any measured current level the corresponding surface temperature $T_2=T$ can be calculated, if $\lambda_{1,2}$ is known.

The "mean effective wavelength" $\lambda_{1,2}$ can be determined by means of any pair of two temperatures [4]. Since $\lambda_{1,2}$ varies slightly with temperature $(\lambda_{1,2}(T))$ some iterative measurements and calculations are required.

For a real radiation source the temperature of the surface can be calculated using the modified form of the eq. (25):

$$T=\frac{c_2/\lambda_{1,2}}{ln\left[\frac{\varepsilon\cdot\tau_f\cdot I_{cal}}{I}\left(e^{c_2/(\lambda_{1,2}\cdot T_{cal})}-1\right)+1\right]} \quad (26)$$

where ε and τ_i are the emission coefficient of the surface and the correction of the transmittance of the media between the source and detector, respectively. In practical application the calibration of pyrometers as well as IR-cameras is performed using a more straightforward procedure, which will be explained later.

The emissivity of a surface depends on its temperature and wavelength, as well as on its roughness and state of oxidation. This fact makes it difficult to specify the emission coefficient of a surface accurately. One method of resolving this problem is the two colour pyrometry. The basic idea is that, if the emissivity is not wavelength dependent, then taking a ratio of radiation intensities at two different wavelengths should eliminate the emissivity. Therefore the two colour technique is also called the intensity ratio method. A detailed description of two colour pyrometry is given in different documents [1,6].

6. IR-thermography

As it is mentioned before pyrometers are used only for the measurement of the local temperature of object surfaces. In order to measure the temperature distribution of the whole surface, IR-cameras with more complicated set-up are necessary. For both pyrometers and IR-cameras the same basic relations and calibration techniques are applied for the determination of the surface temperature from the measured thermal radiance. Therefore all basic equations (eqs. (1) - (26)) are also valid for IR-cameras.

6.1 Scanning and imaging

The thermal radiance of each point of the target has to reach the surface of the IR-detector. The scanning and imaging are performed using two different basic techniques: Image scanning technique and focal plane array (FPA) technique.

6.1.1 Image scanning IR-cameras

Image scanning IR-cameras have a single detector. Using opto-mechanical scanners the radiance intensity of each object surface point is detected successively (**Fig. 10**). To achieve a high image frequency (50-60 Hz) the scanning has to be fast. Since the accuracy of the temperature measurement and the image quality are very essential, the detector properties have to meet the requirements of high scanning speed. Therefore mainly quantum detectors with a response time of several microseconds are used in image scanning IR-cameras. But high frequency imaging reduces the radiance intensity on the detector. Especially at low signal intensity the noise level of detectors has an strong influence on the measurement accuracy. Quantum detectors have a permanent noise level, which depends on the detector temperature. A negative influence of the detector noise on the accuracy of the measurement can only be avoided by detector cooling.

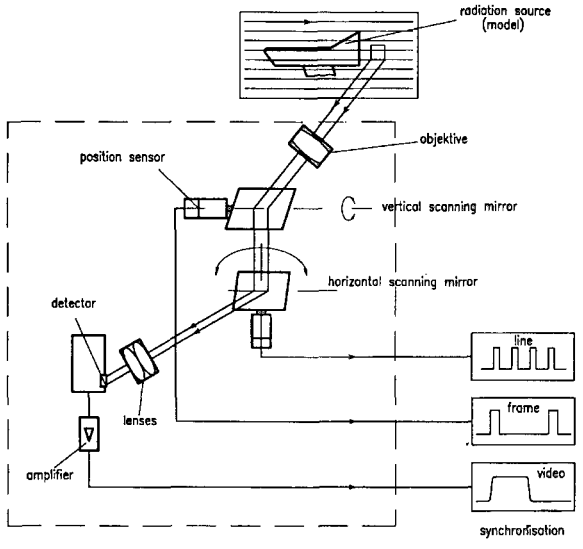

Figure 10. Image scanning of an IR-camera

Usually spinning mirrors or refracting prisms are used for scanning. The inertia of these components, light aberration and the geometrical continuity of the image are key parameters of the scanner components. The line scanning technique, which has a fast horizontal pixel by pixel scanning, finds application in most of the scanning cameras. An IR-frame is created by slower line scanning in vertical direction, which is usually performed at lower speed.

The detector provides an electrical signal corresponding to the infrared image. If the IR-camera use the linear range of the detector, this analogue video signal in the form of voltage or current is proportional to the radiance of the object within the spectral range of the IR-equipment. To yield the radiance intensity distribution at each pixel, synchronisation of the scanning with the radiation beam is necessary. Therefore the deflection of the scanner mirrors or prisms is measured by position sensors. These sensors deliver signals, which mark the begin of lines of the frame. The synchronisation signals can be transmitted to the signal processor separately or in multiplex form. The corresponding temperature to each radiance intensity of each pixel is deduced using calibration curves, which are created experimentally (**Fig. 11**).

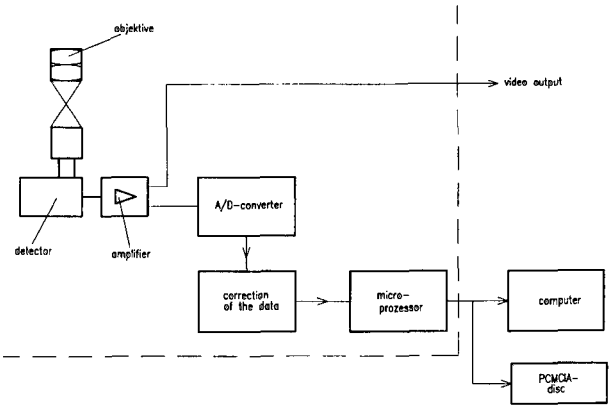

Figure 11. Signal processing of an IR-camera

The analogue output signal of the IR-camera is comparable with the television signal and can be monitored easily. The signal can be divided into steps corresponding to different temperature levels, which are marked on the screen.

For further analysis of the large data field the digitisation of the data is necessary. Fast analogue/ digital converters with a resolution between 8 Bits and 14 Bits are used for this process. The digitised data with a well described structure allows a flexible analysis and correction of the data with respect to emissivity, transmittance, etc. easily.

6.1.2 Focal Plane Array (FPA) IR-cameras

Each moving component of devices has a limited life duration and is sensitive to misalignment. To overcome such problems focal plane array (FPA) detectors have been developed recently. Comparable to CCD-chips of video cameras FPA detectors

consist of several thousands of small detector elements (for example 320 pixel per each of the 240 lines). The thermal radiance distribution of the object is detected simultaneously. Each detector element has to be compensated individually to gain a high image quality. Most of the FPA IR-cameras use quantum detectors, which require active cooling, in order to keep the noise level low. Stirling cycle cooling consisting of two moving pistons and a regenerator is usually used in recent developments.

Last year AGEMA (now Flir Systems) developed a new type of FPA-camera. The detector consists of 76800 microbolometers made of Si-elements coated with a VO_x thermal resistance layer. As we have seen before bolometers are thermal detectors and are operated without cooling. But besides the thermal radiance of the target, the radiation of components inside the camera may be detected by the uncooled detector arrays, which can influence the measurement accuracy. Therefore the inside case temperature is measured at several locations and is used in the automatic re-calibration of the camera at defined time intervals. In addition to avoid any convective heat transfer to the detector elements, they are placed in a vacuum chamber and their temperature is kept close to the ambient temperature using Peltier elements. Even when the response time of bolometers is remarkably longer than quantum detectors, an image frequency of 60 Hz is achievable with this system. The absence of moving parts makes the operation of the Thermovision 570 S IR-camera of AGEMA more comfortable and safely. Although bolometers are not selective with respect to the spectral range, using optical filters this camera is optimised for a spectral range of 7.5-13 μm.

7. Calibration of pyrometers and IR-cameras

Since the radiance of a black body is independent from the surface roughness, the angle of incidence, etc. ($\varepsilon = 1$), black body sources are one of the common calibration devices. One method for realisation of a black body is to develop a perfect absorber by means of some special treatments and surface painting. But this method is limited in the accuracy and temperature range. A second and widely used method is to use a cavity with a very small hole compared to the surface area of the cavity. Due to the multiple reflection of radiation beams inside the cavity, thermal equilibrium is reached after a certain time depending on the cavity wall temperature. Mostly electrical heating technique is used to set different temperature levels in the cavity. Tungsten ribbon lamps consisting of an electrically heated tungsten strip in a glass tube, are also used for the calibration of pyrometers and IR-cameras for the wavelength range up to 2 μm.

As it can be seen in eq. (22) the output signal of the detector of an IR-device is a complex function of the spectral properties of the detector and other optical components. Since an analytical description of this function is very difficult, the relation between the output signal and thermal radiance is determined by calibration data. The output current of the detector can be approximated by the equation:

$$I = \frac{a}{e^{b/T} - 1}. \qquad (27)$$

The black body calibration source is heated to different temperature levels and corresponding output signals (current or voltage) are registered. From the so obtained couples (T_i, I_i) the validation parameters a and b are calculated using the method of least squares approximation. In order to correct the influence of the thermal drift, which may be caused due to the heating of electrical circuits and mechanical components of the camera or change in the ambient temperature, these temperatures have to be recorded during the calibration.

8. Requirements on an IR-system at high enthalpy facilities

The choice of an IR-camera or pyrometer for the application at high enthalpy facilities has different priorities depending on the test duration of the facility. The response time of the IR-system is essential for shock tunnels or impulse facilities. Because of the short test duration of several milliseconds only quantum detectors can be used for the IR-application at these facilities. Even the IR-cameras with quantum detectors are limited with the imaging frequency of 50-60 Hz. Therefore the use of IR-cameras at short duration facilities is only possible by the modification of the system for each special case. Because of their faster response time some pyrometers are more convenient for this application.

At arc jet and induction heated facilities with long test duration of several minutes other aspects become more important. Since these facilities are mainly used for the qualification of thermal protection system (TPS) components, surface temperatures up to 3000 °C are achieved. At such high temperatures gas and solid particles with very different spectral properties can be formed around the test model. Especially the deposition of solid particles on the optical windows may change their transmittance in some spectral ranges remarkably. These phenomena influence also the surface emittance of the model. In the transition phase of an oxidation process on the model surface the emissivity may change significantly and lead to problems in the measurement accuracy of the surface temperature by a pyrometer and an IR-camera.

The operation of arc jet and induction heated facilities is coupled to high voltage, high current and strong electromagnetic fields. Besides its possible influence on the measurement device, such environments require special care concerning the safety of the facility operation team. Therefore a flexible remote control of the IR-systems in long duration high enthalpy facilities is very important.

Based on the facts mentioned above the specification of an IR-camera or a pyrometer for high temperature measurements could be performed according to following aspects:

- **Detector properties**

The differentiation of the Planck's relation (eq. (13)) leads to the so-called Wien's law:

$$\lambda_{max} = \frac{2898}{T} \ [\mu m]. \qquad (28)$$

This relation states that the maximum of the spectral radiance moves to shorter wavelengths as the temperature increases (**Fig. 12**).

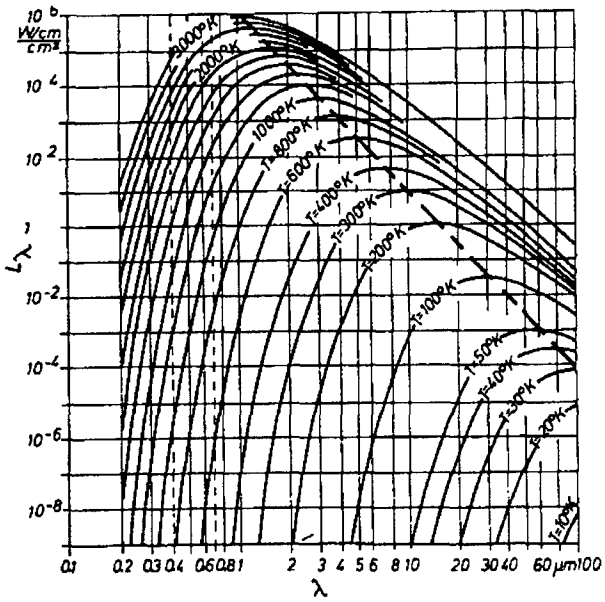

Figure 12. Black body spectrum at different temperatures [7]

According to Wien's law the maximum spectral radiance at a surface temperature of 290 K is around 10 μm. At high surface temperatures around 2800 K a detector with a spectral range around 1 μm would provide the maximum output signal. At that point two main properties of the detector are important. The first one is the sensitivity (*S*), which is defined by the relation between the output signal and incident radiance flux. The minimum detectable radiance energy, which is equivalent to the noise level of the detector, is called the noise equivalent power (NEP). The detector detectivity (*D*) is the reverse value of NEP (*D* = 1/NEP). Both sensitivity and detectivity of the sensor should have a high value in the chosen spectral range. Material properties, coating and the cooling of the detector define *S* and *D*.

- **Thermal and spatial resolution of the IR-system**

The thermal resolution is the minimum detectable difference between the temperatures of different object elements or between the object and its environment. The spatial resolution is the smallest distance between two detectable neighbour object elements. It is usually defined by the elementary solid angle of the system, which results from the combination of different factors like transfer functions of the optics, electronics and visualization system. Both thermal and spatial resolution of an IR-system should be as small as possible.

- **Transmittance of optical components**

The spectral property of optical lenses and filters combined with the detector behaviour define the complete spectral range of an IR-camera or a pyrometer. As defined in the chapter 4.3 most of the optical glasses with OH-ions have a very low transmittance beyond 3 μm. Because of its several absorption lines around in the spectral range of 1-8 μm any water diffusion into the optical glasses has to be avoided. In the spectral range between 7.5-14 μm special glasses with anti-reflective films have to be used.

- **Transmittance of the atmosphere**

As it is described in the chapter 4.2 the atmosphere inside and outside the test chamber have to be considered by the specification of the spectral range of the camera.

- **Radiance of foreign surfaces**

In the case of any other facility component with a significant thermal radiance in the chosen spectral range, the measurement accuracy can be influenced by this foreign radiance source. A proper choice of the spectral range, objective angle and placement

of the camera could allow to overcome this problem.

- **Emissivity of the model surfaces**

The spectral emittance of different materials can vary significantly. Therefore it is very difficult to cover the spectral behaviour of all materials with one IR-system. Since the long duration high enthalpy facilities are mainly used for the qualification of TPS-materials the spectral emissivity of these materials in the high temperature region could be used in the specification of the spectral range of the IR-system.

- **Safety aspects**

As mentioned before the high voltage-current level and strong electromagnetic fields of arc jet and induction heated facilities require special care of the personal safety. Therefore a flexible remote control of the IR-devices is an important aspect for the specification.

9. Application different of pyrometers and IR-cameras at LBK

The arc heated facility LBK consisting of two test legs L2K and L3K has been playing an important role in the qualification and testing of TPS components and materials in the frame of different space programmes like Hermes, X-38, etc. The test facility L2K with a maximum electrical power of 1.4 MW is equipped with a Huels type arc heater and allows to achieve cold wall heat flux rates up to 2 MW/m² at stagnation pressures up to 150 hPa. The L3K facility has a segmented arc heater with a 6 MW power supply. Models with a size of 300 mm (W) x 300 mm (L) x 50 mm (H) can be tested in this facility. In the stagnation point configuration cold wall heat flux rates up to 4 MW/ m² at pressures up to 400 hPa can be set on models with a diameter of 150 mm. A detailed description of the facility can be found in several documents [8,9].

9.1 Measurement configuration of IR-systems at LBK

Based on the fact that mainly high surface temperatures from 500°C up to 2600°C are achieved in LBK and specification criteria for an IR-system defined in the chapter 8, IR-devices with a spectral range in the near IR-region are more convenient for this facility. The temperature measurement using an unique pyrometer or IR-camera in a wide range between the room temperature and temperatures up to 3000°C with a high accuracy is very difficult. Therefore several spectral pyrometers with different measurement ranges are installed at LBK. All these pyrometers have a spectral range around 1 µm. In addition to spectral pyrometers two two colour pyrometers with a measurement range of 800-2000°C and 900-3000°C are used to perform complementary measurements and to determine the emissivity of materials with grey surface properties. Compared to a pyrometer the hardware and software of an IR-camera is more complicated and expensive. Therefore the type and variety of these systems are limited. As mentioned before the safety of the facility operation team of LBK is a very important issue. As a result of these aspects a FPA-camera with an uncooled bolometer detector and remote control system (AGEMA TV 570 S) has been used at LBK. The spectral range of the camera with a measurement range of –20°C–2000°C is

7.5-13 μm. In order to achieve high accuracy the calibration of the camera has been performed for three different measurement ranges (-20-120°C, 80-500°C, 350-2000°C). **Figure 13** shows the experimental set-up to measure the model surface temperature in LBK using pyrometers and IR-camera.

As shown in Fig. 13 the front surface temperature of the stagnation point model is measured with pyrometers placed outside the test chamber via an optical window. The measurement of the rear surface temperature is also important to investigate the influence of the flow radiation and temperature gradient in the sample. Thermocouples integrated in the insulator part behind the sample have been used to measure the rear surface temperature. But at high temperatures beyond 1600°C chemical interactions between particles released from the sample rear surface and thermocouple limit reliable temperature measurements. Therefore a pyrometer with miniaturized optics was developed for the measurement of sample rear surface temperature [10]. Since the test chamber is exposed to high thermal loads at low pressure levels the pyrometer is placed outside the test chamber and the radiation is transferred to the pyrometer via a fibre-optics connection. The miniaturized optical system is shown in the **Fig. 14.** A lens with a focal length of $f = 20$ mm is used. The distance between the lens and the sample rear surface is about 70 mm. A protective glass is used in front of the lens, in order to avoid any hazard to the lens in the case of a crack in the sample causing high enthalpy flow into the system. The fibre-optics inside the test chamber have a metallic coating and is applicable at temperatures up to 400°C.

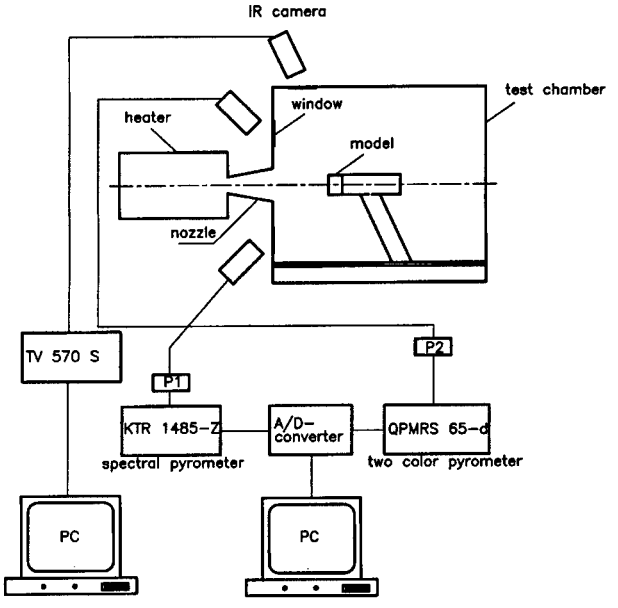

Figure 13. Experimental set-up of pyrometers and IR-camera at LBK

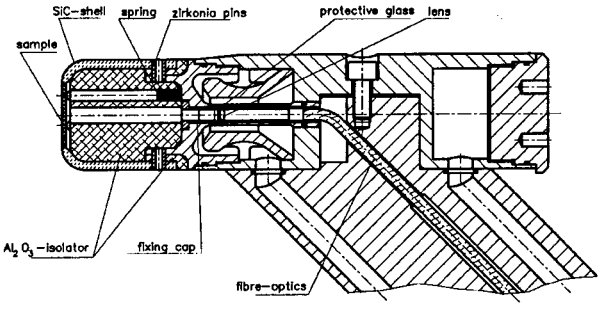

Figure 14. Miniaturized pyrometer optics integrated in the stagnation point model holder

9.2 Comparative temperature measurements in LBK

Since several parameters like the change of the emissivity due to the oxidation processes on the model surface, modification of the transmittance of the optical windows and test ambient during a test in LBK, comparative measurements using different pyrometers and an IR-camera is very important.

During comparative measurements of the front and rear surface temperatures of a stagnation point model with integrated miniaturized optics several temperature levels were set in L2K. The surface temperature of the sample was varied setting different reservoir flow conditions or moving the sample holder in axial direction to different distances from the exit of a conical nozzle. An unexpected behaviour between surface temperatures measured using the miniaturized pyrometer (rear surface) and the spectral pyrometer (front surface) were noticed (**Table 1**). The measured rear surface temperature is higher than the front surface temperature.

front surface	**front surface**	**rear surface (VL 70/8)**
spectral pyrometer	**two colour pyrometer**	
T_{s1} [°C]	T_{q1} [°C]	T_{q2} [°C]
1176	1180	1222
1318	1330	1360
1381	1395	1437

Table 1. Surface temperatures measured on a SiC sample in L2K

Because of some heat losses from the sample to the fixing SiC-shell the front surface temperature has to be higher than the rear surface temperature. In radiation equilibrium the heat flux to the sample can be described as:

$$\dot{q} = \varepsilon \cdot \sigma \cdot \left(T_s^4 - T_\infty^4\right) + \dot{q}_{loss} . \qquad (29)$$

Here $\sigma\left(= 7.56042 \cdot 10^{-16}\, j/\left(K^4 \cdot m^3\right)\right)$, T_s and T_∞ are the Stephan-Boltzmann constant, the surface temperature and the temperature of the environment, respectively. Especially the ambient temperature in the test chamber is negligible compared to the sample surface temperature in the stagnation point configuration. If we neglect the heat loss the equation (29) takes the form:

$$\dot{q} \approx \varepsilon \cdot \sigma \cdot T_s^4 . \qquad (30)$$

The differentiation of this equation leads to the relation

$$\frac{d\dot{q}}{\dot{q}} \approx 4 \cdot \frac{dT_s}{T_s} . \qquad (31)$$

Equation (31) shows that a temperature change of 1% causes nearly 4% change in the equilibrium heat flux rate. Similarly an error in the temperature measurement causes about a four times higher error in the heat flux determination.

The isolation material behind the sample has high and different temperature levels along its length and causes additional radiation, which can increase the radiance at the entrance of the miniature optics. Therefore a small aperture stop was installed between the lens and the fibre-optics and the inner surface of the optics tube was coated with a black layer, in order to eliminate the influence of the foreign illumination and reflected light on the results. After the new calibration of the pyrometer with miniaturized optics using a black body, additional control measurements were performed in the L2K-facility. A significant improvement was achieved due to this modification (**Table 2**).

front surface		rear surface (VL 70/8)
spectral pyrometer	two colour pyrometer	
T_{s1} [°C]	T_{q1} [°C]	T_{q2} [°C]
1059	1055	1062
1115	–	1113
1120	–	1120
1225	–	1231
1262	–	1263
1306	–	1306
1295	1288	1296

Table 2. Surface temperatures measured on a SiC sample in L2K with modified miniaturized optics VL 70/8

According to theoretical estimations and some experimental results the front surface temperature should be about 30-50°C higher than the rear surface temperature. Further investigations are necessary to achieve higher accuracy of the temperature measurement on the rear surface of the sample using the pyrometer with miniaturized optics.

9.3 Tests to investigate the influence of external windows and impurities

Since surface temperature measurements using pyrometry are mostly performed by keeping the pyrometer outside the test chamber via optical windows, the radiance of the model surface is partly weaked due to the window. The type and geometry of the optical glass can vary depending on pyrometer characteristics and test conditions in the test chamber. Therefore it is more convenient to consider the influence of the window during control measurements first after the calibration. It avoids repeated device calibrations in the case of the replacement of the window. **Table 3** shows the influence of a quartz-glass (suprasil) with a thickness of 10 mm on the temperature measurements on a SiC-sample in an oven.

spectral pyrometer		two colour pyrometer	
without window	with window	without window	with window
T_s [°C]	T_s [°C]	T_q [°C]	T_q [°C]
939	932	943	942
1016	1009	1024	1023

Table 3. Measured temperatures of a black body using a quartz window

During the influence of the quartz window on the temperature measured using the two colour pyrometer is negligible, this window causes a temperature decrease of about 0.7% in the temperature determined with a spectral pyrometer.

Impurities on the window could also cause some uncertainties in the temperature measurement. Especially water has strong absorption bands in the infrared spectrum. A water droplet with a diameter of about 5 mm was placed on the quartz tube in the radiation beam range and surface temperature of a SiC-sample heated in an oven was measured with both spectral and two colour pyrometers via this window. The results are listed in the **Table 4**.

spectral pyrometer		two colour pyrometer	
dry window	wet window	dry window	wet window
T_s [°C]	T_s [°C]	T_q [°C]	T_q [°C]
932	926	942	942
1009	1003	1023	1023

Table 4. The influence of a water droplet on temperatures measured with spectral and two colour pyrometers via a quartz window

Because of the two narrow band pass filters of the two colour pyrometer at the wavelengths of 920 nm and 1040 nm and the constance of the low water absorption at these two wavelengths no temperature change was caused due to the water droplet placed on the quartz-window. Same water droplet caused a temperature decrease of about 0.6% in the temperatures measured with a spectral pyrometer. The reason may be the absorption of the radiation due to water in a relatively broader wavelength range of 800-1100 nm of the spectral pyrometer.

9.4 Angle dependence of temperature measurements

As mentioned before the geometry of the heater and the test chamber of high enthalpy facilities allow to perform temperature measurements of a model in the stagnation point test configuration of high enthalpy facilities only under some angle between the axis of the sample holder and the pyrometer axis. The measurements in LBK-facilities are performed in an angle range of between 30° and 60°. To investigate the influence of the angle on the temperature measurement a SiC-sample was heated in the DLR solar furnace, which allows pyrometer measurements in a wide angle range. The main components of this 15 kW facility are a plain mirror (heliostat) and a large concave mirror (concentrator) [11]. The concentrated solar radiation is deflected to the test room located off-side. The concentrator consists of various concave reflector elements with different focal lengths. Energy flux densities up to 2500 kW/m² in a homogeneous core with a diameter of 80-120 mm can be achieved in this facility. Measurements at different angles (α) between the axis of the sample surface exposed to the sun beam and the pyrometer axis were performed. Measured temperatures with spectral and two colour pyrometers are listed in **Table 5.**

While the temperature T_s measured with the spectral pyrometer showed a weak dependence on the measurement angle, a remarkably high temperature increase was noticed in the temperature T_q measured with the two colour pyrometer at the angle of 67.5°. The reason of different of two pyrometers has not been clarified yet.

α (°)	T_s (°C)	T_q (°C)
22.5	1003	986
45.0	1003	992
67.5	1006	1049

Table 5. Surface temperatures measured with pyrometers under different angles in the DLR solar furnace

9.5 Different application of the IR-camera at LBK

As mentioned before IR-thermograpy provides a temperature map of the surface and allows a quick judgement concerning the gas surface interaction.

A detailed post-analysis of the measured data and corrections in terms of the surface emissivity and transmittance of the optical windows or the atmosphere can be done using sophisticated software of these systems. The complementary surface temperature measurement using a spectral pyrometer, a two colour pyrometer and an IR-camera in LBK facilities increase the reliability of the experimental data significantly.

Figure 15 shows the measured temperature distribution on a flap model with a gap between the plate and flap representing the hinge line area of the X-38 demonstrators in LBK. The hot structure made of C/SiC is integrated in a water cooled metal model holder. In order to avoid heat losses from the model to the holder an insulation material was used at the interfaces of the model to the holder nose and side plates. Because of its lower radiation cooling and higher catalysis the surface temperature of the insulation material is much higher than the model surface. But it should be mentioned that this IR-picture is produced for the emissivity value of the C/SiC material ($\varepsilon = 0.8$). Since the emissivity of the insulation material in the spectral range of the IR-camera (7.5-13 μm) is around 0.95 the real temperature of the front part is about 280 K lower than the temperature shown in the **Fig. 16**. Another important point is the temperature development in the gap, which is heated due to the high enthalpy gap forced by the pressure difference between the upper and lower surface of the model at 30° angle of attack. Since the gap front and rear walls, which make nearly 90% of its complete radiation surface, have a very small radiation angle, the gap behaves like a black body. Therefore the effective emissivity is larger than 0.85, which would mean a lower gap temperature of the gap compared to the value given in the IR-picture. The data of thermocouples integrated in the gap confirmed this result. This IR-image shows clearly that the flow filed around the model is two dimensional, which was a very important criteria for the test campaign. Although the temperature gradients are smeared as a result of the lateral heat conduction inside the C/SiC material, the measured surface temperature increase in the front part of ramp is directly correlated to the convective heating behind the re-attachment shock on the ramp. Comparative measurement of the surface temperature of a spot on the ramp using spectral and two colour pyrometers with a spectral range around 1 μm provided an emissivity of 0.85 for this wavelength. These results were confirmed with the data of the manufacturer.

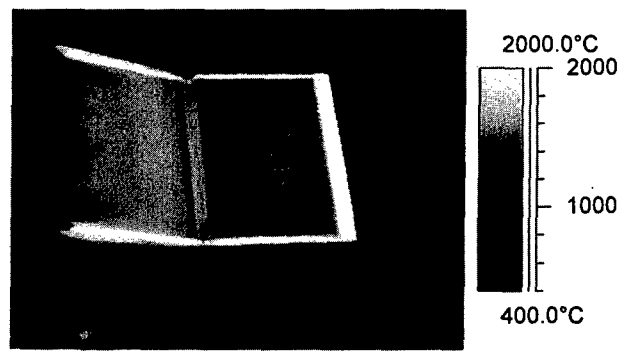

Figure 15. IR-image of a flap model in LBK (flow from right)

During qualification tests of the OHB aerothermodynamic measurement system for the first X-38 demonstrator, the IR-image provided a very important result. As it can be seen on the Fig. 16, the heat flux sensor integrated in the centre of the flexible insulation material (FEI) with a protective coating reaches a lower surface temperature than FEI after a testing time of 25 minutes. It is caused

due to the stronger radiative cooling of the sensor and its heat sink effect resulting from a high heat conductivity and large heat capacity of the substructure. Again a correct emissivity value of each surface component has to be used, in order to deduce the real surface temperature. Fig. 16 shows the correct temperature of the FEI-material for $\varepsilon = 0.8$.

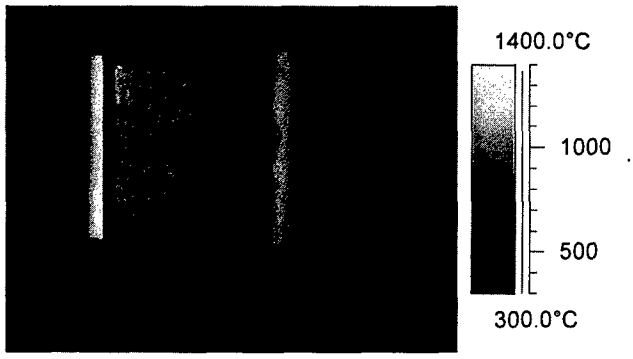

Figure 16. IR-image of the OHB aerothermodynamic system in the flow field of LBK (flow from left)

Figure 17 shows the IR-image of a C/C-SiC model with gap components representing the interface between the nose cap and TPS nose skirt of the X-38 demonstrator in L3K [12,13].

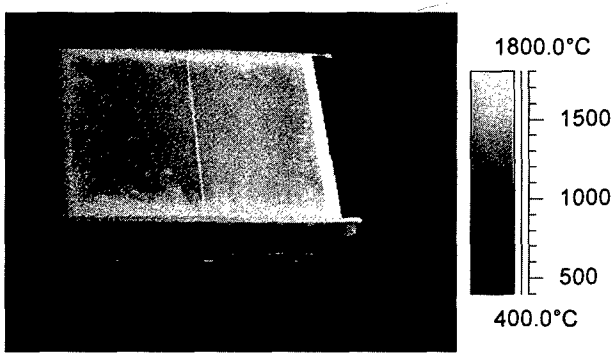

Figure 17. IR-image of the nose cap and nose skirt interface model in L3K (flow from right)

Besides its useful information about the temperature development in the gap region, the IR-image confirms the two dimensionality of the flow. The temperature development of a spot about 10 mm upstream of the gap was measured using a spectral pyrometer and a two colour pyrometer (**Fig. 18**).

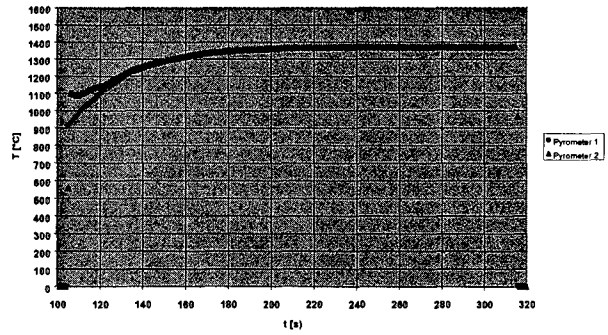

Figure 18. Surface temperature development measured with a spectral pyrometer and a two colour pyrometer on a C/C-SiC model in L3K

The analysis of the measured surface temperatures with pyrometers and IR-camera simultaneously indicates a lower emissivity value of 0.8 of the C/C-SiC material at a spectral range of 7.5-13 μm compared to the emittance of 0.85 around 1 μm, which is the spectral range of the pyrometers.

Another IR image of the same model at a different test configuration showed a similar temperature development in the gap region, but indicated an overheating in the edge region of the model holder (**Fig. 19**). The test was performed at an angle of attack of 50°. It seems that even on a two dimensional model at such high angles of attack some three dimensional flow phenomena occur and lead to severe heat loads. The test was interrupted based on the temperature development measured with the IR-camera. Finally an unexpected damage to the

model and model holder was avoided by means of IR-images.

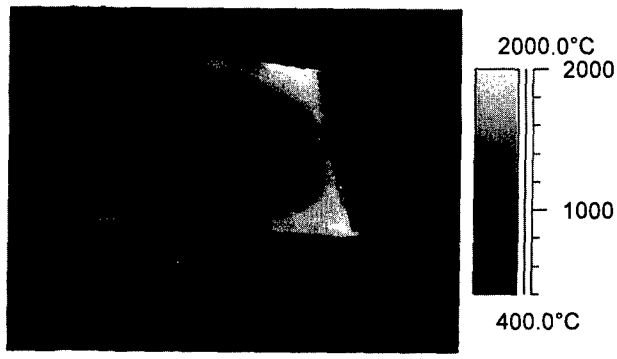

Figure 19. IR-image of the nose cap and nose skirt interface model in L3K (flow from right)

10. Concluding remarks

Although the accuracy and reliability of the surface temperature measurements using pyrometers and IR-cameras have been improved significantly, further development is necessary for some scientific applications. As mentioned before the very short testing time of few milliseconds of shock tunnels and hot shot facilities requires the use of IR-devices with a very fast response time of some microseconds to measure the surface temperature development of test models in these facilities. Another key issue is the determination of the mostly unknown emissivity of materials and the investigation of its selective behaviour. The two and more colour techniques, which are useful tools for the temperature measurements on grey surfaces, are not sufficient to determine the emissivity of selective materials with high accuracy. Complementary measurement of the thermal radiation and surface reflectance of the model could be an important contribution to the improvement of the accuracy and determination of the emissivity.

11. References

[1] Gülhan, A.; *Introduction to pyrometry and comparison of different pyrometer configurations*. VKI Lecture Series on Temperature Measurements, Waterloo, April 22-26, 1996.

[2] Gaussorgues, G.; *Infrared Thermography*. Chapman & Hall, 1995.

[3] TI Technical Journal, Infrared Technology; *Uncooled Infrared Detector Processing*. September-October 1994.

[4] Woerner, B.; *A photoelectric direct current spectral pyrometer with linear characteristics. Temperature, its measurement and control in science and industry*. Volume 5, Editor James F. Schooley. Published by American Institute of Physics.

[5] AGEMA Infrared Systems; *Hintergrundinformationen zu neuen technologischen Entwicklungen auf dem Gebiet der Infrarot-Zustandsüberwachung*. Presseinformation, GE1227P.

[6] Rapp, W.; *Quotientenpyrometer für Temperaturen ab 500°C*. KfK 3371, Kernforschungszentrum Karlsruhe, Juli 1982.

[7] Hunsinger, W.; *Temperaturmessungen mit Strahlungspyrometern*. VDI–Bildungswerk, BW 1456.

[8] Gülhan, A.; *Arc Heated Facility LBK as a Tool to Study High Temperature Phenomena at Re-entry Conditions*. DLR-IB-39113-97A05, 1997.

[9] Gülhan, A.; Esser, B.; *Qualification of TPS-Components in the Arc Heated Facility L3K of DLR.* Proc. of the 3rd European Workshop on Thermal Protection Systems, ESA WPP-141, Noordwijk, pp. 121-130, 1998.

[10] Horstmann, O.; Gülhan, A.; *A pyrometer configuration for measurement of the temperature at the rear side of a TPS-sample.* DLR IB-39113-94A02, 1994.

[11] Becker, M. et al.; *Der Hochflußdichte-Sonnenofen - eine neue Testanlage der DLR.* Einweihung des Sonnenofens am 21. Juni 1994.

[12] Weihs, H.; *Nose Skirt Qualification Test Plan.* TET-DLR-14-TP-3506, 1999.

[13] Gülhan, A.; *Tests on the Feasibility of the Rigid and Flexible Seal Concepts in the Nose Cap Region of X-38.* TET-DLR-21-TN-3514, 1999.